

## Article

# Morphological, Structural and Optical Characterization of Bottom-Up Growth of Ag-WO<sub>3</sub> Core-Shell Nano-Cube Heterostructures

Muhammad A. Imam and Nitin Chopra \*

Department of Metallurgical and Materials Engineering, University of Alabama, Tuscaloosa, AL 35487, USA; maimam@crimson.ua.edu

\* Correspondence: nchopra@eng.ua.edu; Tel.: +1- (205) 348-4153

**Abstract:** A new class of nano-cube core-shell heterostructures containing Ag coating on the top of WO<sub>3</sub> was fabricated. Physical vapor deposition was used to produce WO<sub>3</sub> based nano-heterostructures. All kind of wet toxic chemical process was avoided to make the process simple and contaminant free. Sputtering of WO<sub>3</sub> and a subsequent thermal annealing process was done to create nano-cubes of WO<sub>3</sub>. After that, sputtering of Ag was performed to form the Ag-WO<sub>3</sub> core-shell nano-heterostructures (CSNH). The CSNHs were characterized using field emission scanning electron microscopy (FESEM), energy dispersive spectroscopy (EDS), X-ray diffraction analysis (XRD) and UV-vis spectroscopy. The morphologies, elemental analysis, interfaces, crystallinity, phases, and chemical compositions were analyzed. The bottom-up growth of WO<sub>3</sub> nanocubes was studied using different time periods at 900°C. Ag coating was also studied before and after annealing. Finally, an optical property (band gap) was also analyzed using Tauc plot derive from absorption spectra. The tailoring the band gap of WO<sub>3</sub> from ~2.9eV to ~2.45 eV was observed while Ag-WO<sub>3</sub> CSNH formed.

**Keywords:** nano-cube; heterostructures; bottom-up growth; electron microscopy; bandgap; Ag-WO<sub>3</sub>

## 1. Introduction

In recent years, manipulation and fabrication of oxide-based core-shell heterostructures and the creation of interface among transition metal oxides have presaged the latest era of materials research. It is enabling an exceptionally discrete set of coinciding material properties to be pooled with an escalating degree of experimental control. Transition metal oxides are also known as semiconducting materials having a wide band gap, which can be tuned while being used as heterostructures. To tune the band gap facilitates rapid charge transport [1] and unique photonic[2] properties which are not possible with a single component or similar structures. Transitional metal oxide heterostructures systems have already exhibited such diverse application as a photocatalyst, photodetectors, FET, LED , gas sensor, chemical sensor, super capacitors, solar cells and surface acoustic wave filters [3-7]. To completely utilize these affluence; it is required to comprehend and be able to control the physics on the smallest scales, creating the exploitation of nanoscale heterostructures. Some of these avenues have already been explored for different applications.

Solar energy is a clean and renewable source of energy. It has acknowledged for photo-degradation of environment pollutants [8-13]. Various metal oxide nanostructures are used for photocatalytic applications [14-18]. The photochemistry of oxide nanoparticles has established a significant concern due to their particular photocatalytic behavior [17,19,20]. Apart from this photocatalytic behavior, numerous researches have been conducted on metal oxide semiconductor (such as TiO<sub>2</sub>, In<sub>2</sub>O<sub>3</sub>, WO<sub>3</sub>, ZnO, SnO<sub>2</sub>,) thin film coated gas sensors to detect industrial effluents NH<sub>3</sub>, H<sub>2</sub>CO, H<sub>2</sub>S, ethanol and methanol [21-24]. In recent times, metal oxide nanostructures (such as nanoparticles, nanotubes, nanowires, nanobelts) have proved to be suitable for chemical sensors as



they have a distinctive surface, small-size, and quantum effects. Nanostructures based on transitional metal oxide characteristically have a quicker response due to their very high surface-to-volume ratios. Some literature drew attention towards metal oxide heterostructures, for example, ZnO coated with Ag, WO<sub>3</sub>, Zinc Tin Oxide (ZTO) and CdS for better photocatalytic and gas sensor application. Similarly, CuO/Co<sub>3</sub>O<sub>4</sub> showed better photocatalytic behavior than simple metal oxide (CuO) nanostructures [3, 5, 17, 25-28]. For better chemical sensing and catalysis, CNT coated Ni/NiO core-shell heterostructures were also studied in the literature [26]. Ag-AgBr coated Al<sub>2</sub>O<sub>3</sub> heterostructure was reported for photo-degradation of industrial contaminants [29]. Ag-coated ZnO, WO<sub>3</sub>, and MnO<sub>2</sub> were also explored for photocatalytic applications, better chemical sensor and supercapacitors respectively [7, 25, 27, 28]. Among the various oxides, WO<sub>3</sub> has a graphene-like 2D layered structure [30] with wide band gap (~2.8eV) [31]. This limits its optical responsivity in the visible region of the electromagnetic spectrum for photocatalytic application. Hence, bandgap tuning of WO<sub>3</sub> is essential since it governs the energy necessary for the generation of electron-hole pairs. Metal particles such as Ag act as localized surface plasmons (LSP), which attribute electromagnetic waves joined to the combined oscillations of electrons [32]. Ag can tailor the band gap of WO<sub>3</sub> in such a way that the spectral response of Ag-coated WO<sub>3</sub> heterostructures can be extended to the visible region.

Metal oxide heterostructures drew attention due to their low cost and better photocatalytic/sensing behavior than precious materials. It can be synthesized using a wide array of methods including solution synthesis, gas phase growth i.e. physical/chemical vapor deposition (PVD/CVD), flame synthesis, air oxidation. Gas-phase methods, specifically CVD and pulsed laser deposition (PLD), were used to maintain atomic level control of stoichiometric ratio and perfect particular site deposition. Due to their high cost and low throughput, these processes are not accepted widely for general industrial applications. Sputtering deposition, another tradeoff gas phase technique, have been considered because of its potential for assembling heterostructures, comparably lower cost and high throughput than other gas phase methods [33].

Here, we report a new choice of core-shell nano-heterostructures (CSNH) of Ag-coated WO<sub>3</sub> (Ag-WO<sub>3</sub>) CSNH. Physical vapor deposition (PVD) technique (sputtering) is used to obtain a thin layer, and a subsequent thermal annealing process was used to grow the Ag-WO<sub>3</sub> CSNH. All traditional hydrothermal processes were avoided to keep the process simple and reduce the use of toxic chemicals. The nanostructures were extensively characterized for their phases, crystal structures, morphologies and elemental analysis. A field effect scanning electron microscope (FESEM) was used to understand the growth mechanism and morphology. Energy dispersive x-ray spectroscopy (EDX) was performed to confirm the elemental analysis. X-ray diffraction analysis was also conducted to comprehend the phase and crystalline properties of the materials. Along with this, UV-vis was evaluated to calculate the band gap energies of Ag-WO<sub>3</sub>, which is optically more viable than WO<sub>3</sub> for photocatalytic application.

## 2. Materials and Methods

### 2.1 Materials

Silicon (111) wafers were acquired from IWS (Colfax, CA), Isopropyl alcohol (IPA) from Sigma-Aldrich (St. Louis, MO), and Deionized (DI, 18.1 MΩ·cm) water was obtained using a Barnstead International DI water system (E-pure D4641). Both WO<sub>3</sub> and Ag targets (2 in. diameter) were purchased from AJA International (North Sitate, MA). PVD was performed using an AJA International (North Sitate, MA) Orion 3 sputtering system. Thermal annealing was conducted in a box furnace (GMF-110) purchased from MTI Inc. (Redmond, CA). Hexane was used as a solvent for ultra-sonication which was procured from Sigma-Aldrich (St. Louis, MO).

### 2.2. Growth of WO<sub>3</sub> Nano-cubes

A 4" silicon wafer was cleaned using IPA and washed with deionized water. After drying the Si wafer, it was placed into the AJA International (North Sitate, MA) Orion 3 sputtering system. The



operating condition for 300 nm thin film of growth was maintained in a high base vacuum pressure of  $2 \times 10^{-7}$  torr. Sputtering of  $\text{WO}_3$  was led using RF power source at 50 W, 150 V with  $6.54 \times 10^{-3}$  torr working pressure. On top of that, 25.1 sccm Ar flow rate, and 25 rpm substrate rotation speed was maintained at a deposition rate of  $0.2 \text{ \AA/s}$  recorded by a quartz thickness monitor. After sputtering of  $\text{WO}_3$  thin film on Si wafer, it was placed in a crucible and air annealed at  $\sim 900^\circ\text{C}$  for 180 min, 240 min and 300 min in a box furnace. After thermal annealing, the furnace was then cooled naturally in the air. Approximately, the  $2 \times 2 \text{ cm}^2$  area of a silicon wafer containing  $\text{WO}_3$  nanocubes was ultra-sonicated using hexane as a solvent to prepare a solution for UV-vis.

### 2.3. Sputtering of Ag onto $\text{WO}_3$ Nano-cubes

The sample of  $\text{WO}_3$  nanocubes on Si wafer was loaded into the sputtering chamber. The high base pressure of the chamber was pumped to below  $2 \times 10^{-7}$  torr. Sputtering of Ag was implemented using a DC power source at 15 W, 750 V with  $6.54 \times 10^{-3}$  torr working pressure. Ar flow rate was maintained 25.1 sccm in the chamber with 25 rpm substrate rotation speed. The sputtering rate was  $0.6 \text{ \AA/s}$  recorded by a quartz thickness monitor. The subsequent heterostructures are stated to as Ag- $\text{WO}_3$  core-shell nano-heterostructures (CSNH). Approximately, the  $2 \times 2 \text{ cm}^2$  area of a silicon wafer containing Ag- $\text{WO}_3$  CSNH was ultra-sonicated using hexane as a solvent to prepare a solution for UV-vis before and after 60 min of annealing at inert atmosphere (Ar). The figure, 1 illustrates the schematic fabrication process of CSNH.

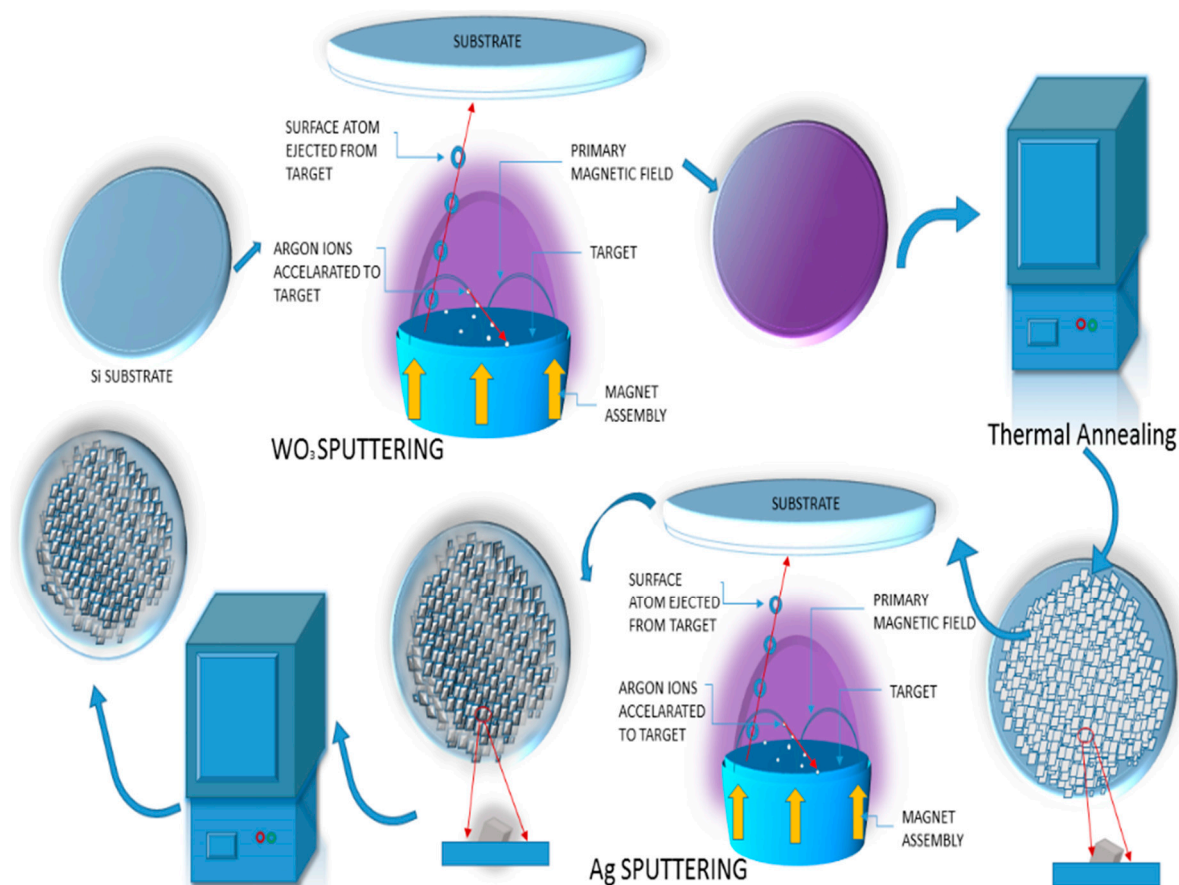


**Figure 1.** Schematic representation of step-by-step fabrication of Ag- $\text{WO}_3$  CSNH



### 2.4. Characterization Methods

A field emission scanning electron microscopy (FESEM, JEOL-7000, equipped with an Oxford EDX detector) was used for morphological characterization and energy-dispersive X-ray spectroscopy (EDX). Philips X'Pert-MPD X-ray Diffraction (XRD) system was used for phase and crystal structure analysis. UV-vis spectroscopy was implemented (absorbance spectra) using an Ocean Optics USB 4000 spectrometer (Dunedin, FL) equipped with DH-2000 UV-vis-NIR light source. The absorption coefficient is defined by the Beer-Lambert's law as  $\alpha(\nu) = \frac{2.303 \times Abs}{d}$ , where abs and d are the absorption and thickness of the sample holder. Tauc plots were plotted by assuming direct band gap transition and plotting  $(\alpha h\nu)^{1/n}$  vs.  $h\nu$  where  $n=1/2$ . The direct band gap were acquired from extrapolating the straight portion of the plot of  $(\alpha h\nu)^2$  versus  $h\nu$  on X- axis at  $\alpha = 0$ .

### 3. Results and Discussion

The figure, 2 represents the FESEM micrograph of  $WO_3$  after each step including as sputtered (Figure,2A) and after annealing at  $900^\circ\text{C}$  for different time periods (Figure,2B-2D). The formation of nano-cube  $WO_3$  was evident from the FESEM images (Figure,2B-2D). Thermal process directly enhances the formation of nano-cube  $WO_3$  from the sputtered  $WO_3$ . This is a bottom-up growth of nanoparticles – the vapor-solid (VS) growth mechanism drives this growth process [33]. The diameter of  $WO_3$  nanocubes was varied from  $\sim 90\text{nm}$  to  $\sim 340\text{ nm}$  (Figure, 2E). The figure,2F represents the EDS analysis of growth particle to confirm the elemental analysis. From the spectrum, Tungsten (W) and Oxygen ( $O_2$ ) peak confirm the growth of  $WO_3$ .

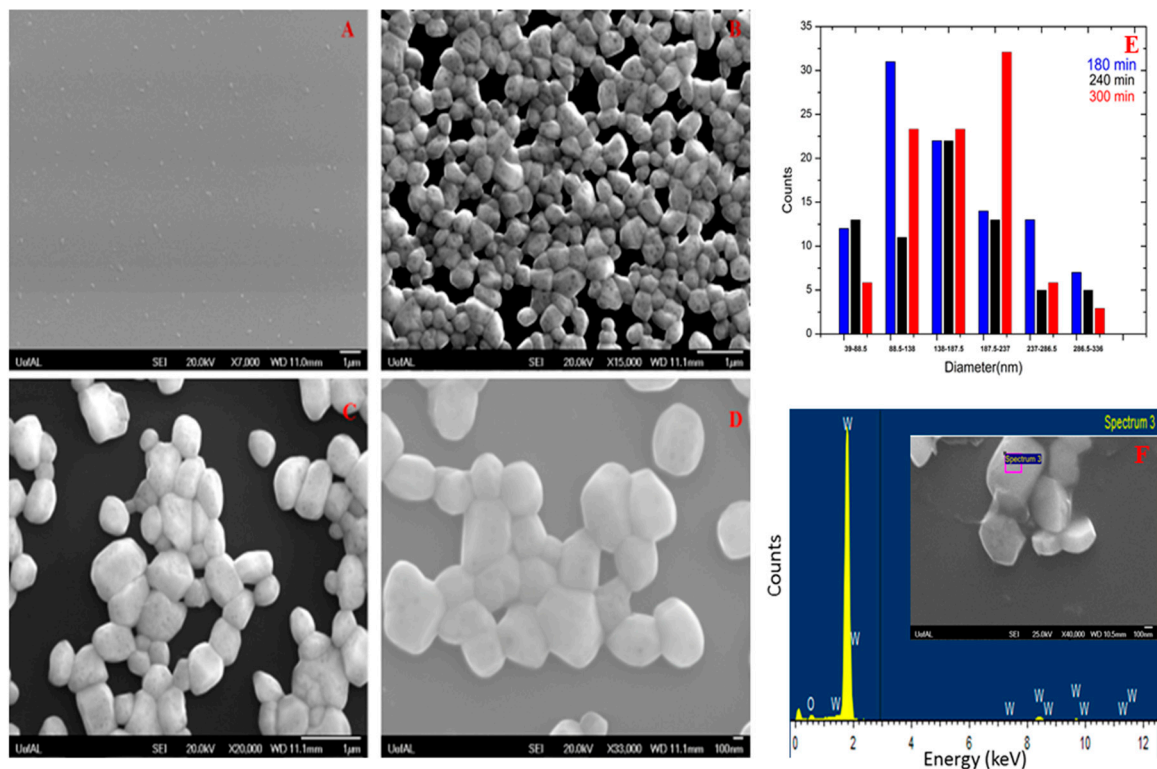


**Figure 2.** FESEM micrograph of  $WO_3$  A. As sputtered, annealing at  $900^\circ\text{C}$  B.180 min C.240 min D. 300 min E. Particle size distribution F. EDX based elemental analysis of  $WO_3$

The figure, 3 shows that FESEM image of Ag- $WO_3$  before (Figure, 3A) and after annealing (Figure, 3C) and their corresponding EDX spectrum (Figure, 3B, and 3D) respectively. From the EDX spectrum, the presence of Ag was confirmed. After annealing, Ag coating was revealed on the edge of the  $WO_3$  (Figure, 3C).



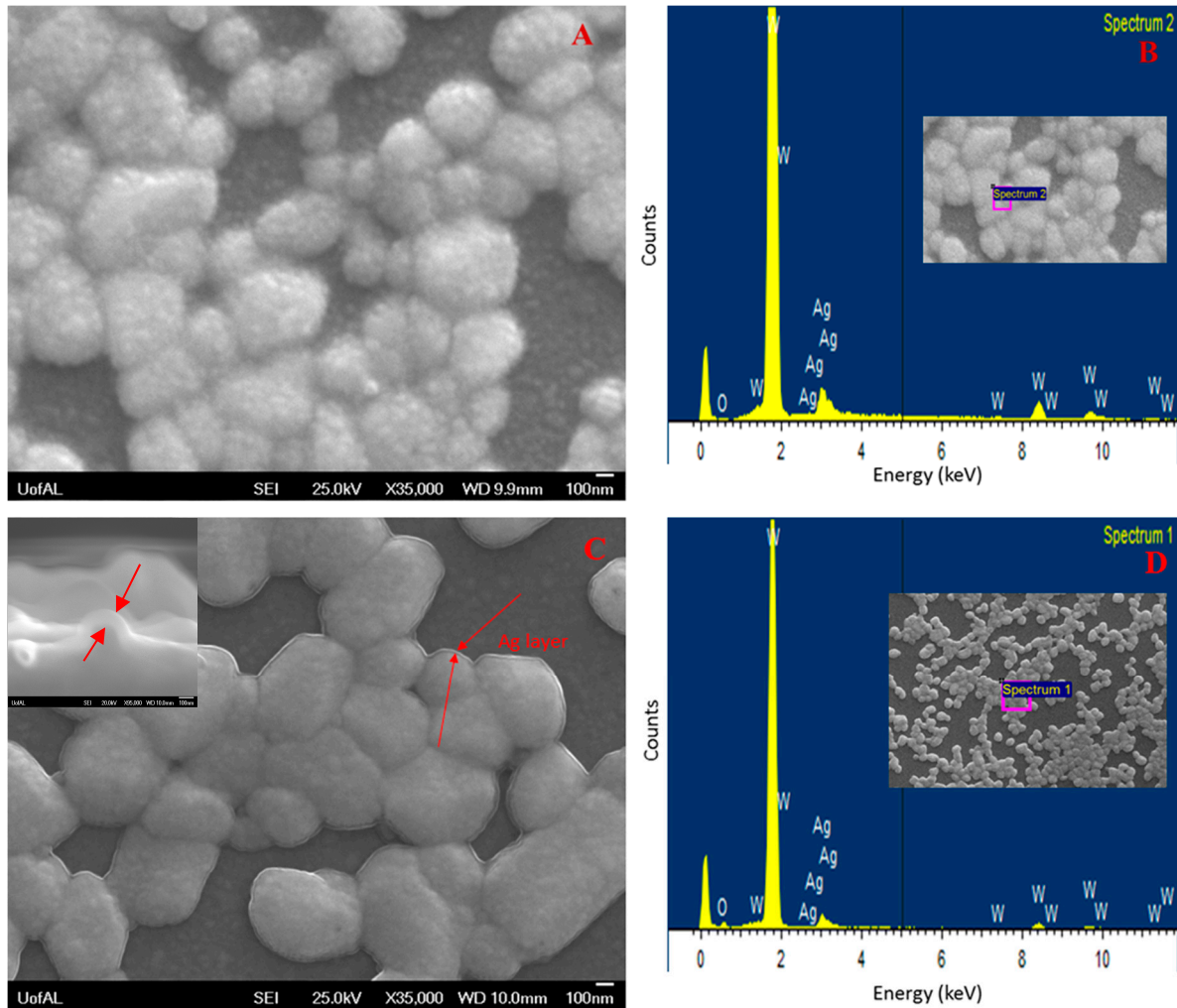


**Figure 3.** FESEM micrograph of Ag-WO<sub>3</sub> CSNH A. Before annealing B. Corresponding EDX based elemental analysis C. After annealing (300°C for 60 min in Ar atmosphere) D. Corresponding EDX based elemental analysis

The figure, 4, demonstrates the XRD results of WO<sub>3</sub> after sputtering and different annealing time. As sputtered WO<sub>3</sub> (Figure, 4.A) shows amorphous characteristics of WO<sub>3</sub>. Only Si peak (PDF # 80-0018) was identified as Si was used as a substrate. But after annealing at 900°C for different time periods, the structure started becoming crystalline and monoclinic WO<sub>3</sub> (PDF # 76-1134) was found. No significant change was observed in phase and crystallinity after annealing in different time periods.



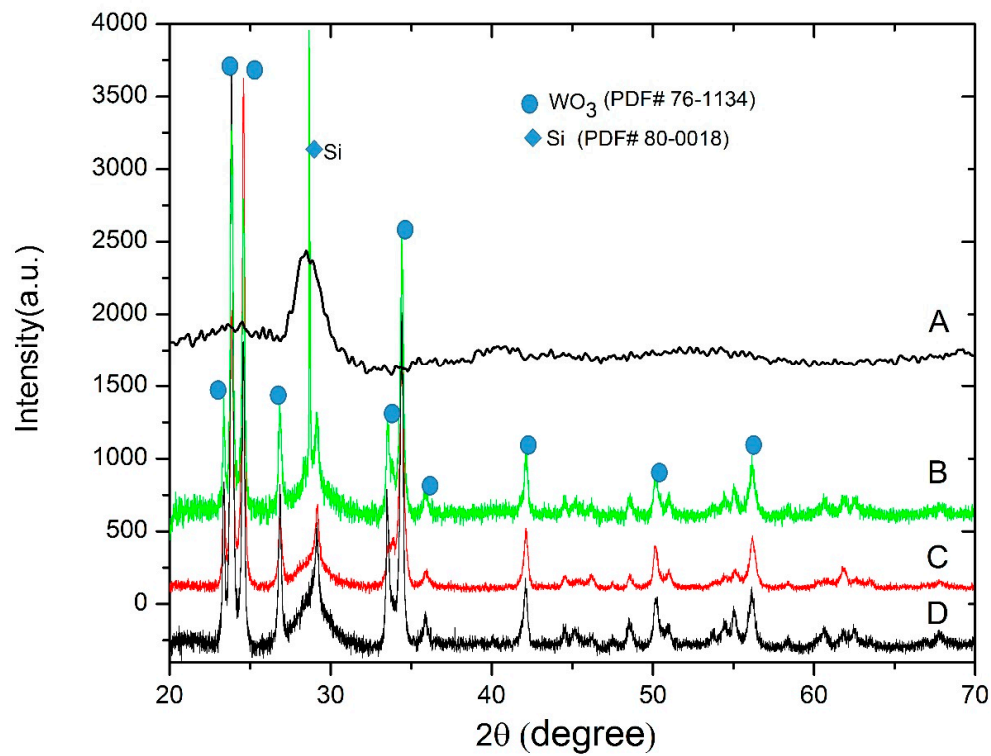


**Figure 4.** XRD patterns for WO<sub>3</sub> A. As sputtered, annealing at 900°C B.300 min C.240 min D. 180 min

After coating with Ag on the WO<sub>3</sub>, XRD was performed again to confirm the phase and crystallinity before and after annealing (Figure, 5B, and 5C). A clear peak of Ag (PDF # 76-1134) was observed after coating with Ag. The significant change of Ag peak was identified after annealing because of better crystallinity.



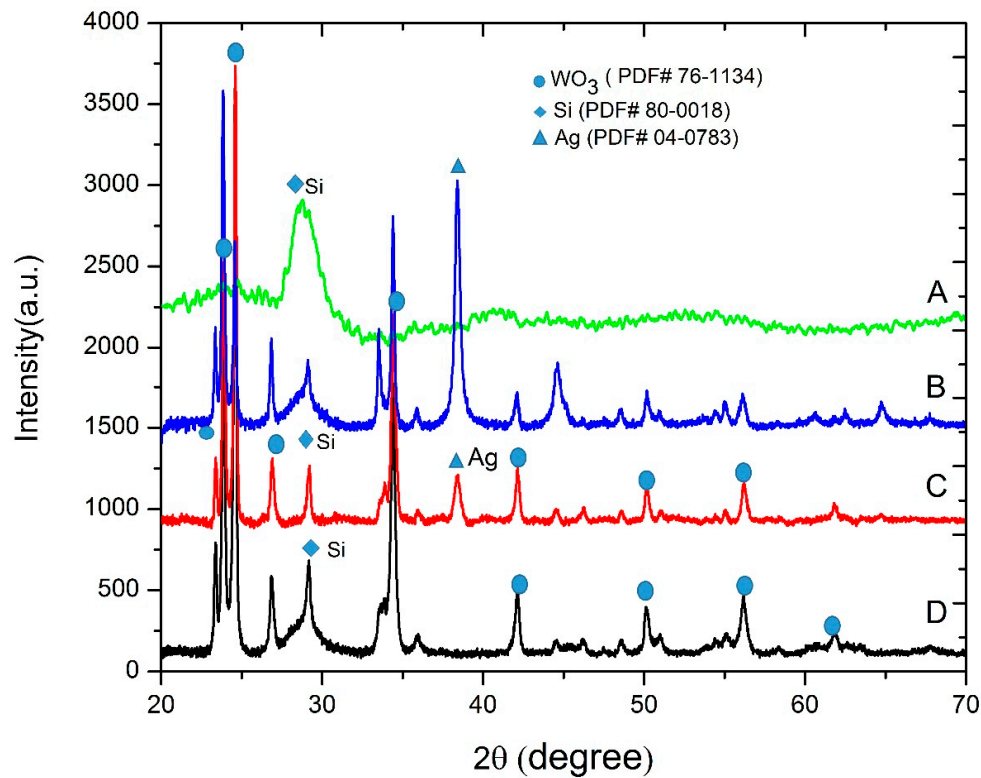


**Figure 5.** XRD patterns of the A. As sputtered WO<sub>3</sub>, B. Ag-WO<sub>3</sub> annealed for 60 min at 300°C, C. Ag-WO<sub>3</sub> before annealing D. Annealed WO<sub>3</sub>.

The figure, 6 shows the UV-Vis absorption spectra of the WO<sub>3</sub> (Figure, 6A), Ag-WO<sub>3</sub> before (Figure, 6A) and after (Figure, 6A) annealing. It was observed that there is a lot of changes in major excitation absorption peaks compared to the WO<sub>3</sub> (~250 nm) and Ag-WO<sub>3</sub> (before ~275 nm and after annealing ~280 nm).

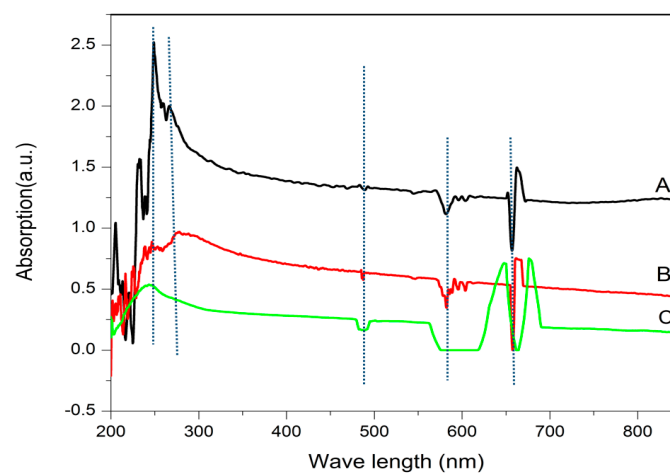


**Figure 6.** UV-vis absorption spectra of WO<sub>3</sub> (A), Ag-WO<sub>3</sub> before (B) and after annealing (C)



The direct band gap of the CSNH (Figure, 7) was estimated from Tauc plots of  $h\nu$  versus  $(\alpha h\nu)^2$  for the absorption coefficient  $\alpha$ . The band gap of  $\text{WO}_3$  was calculated  $\sim 2.9$  eV which matched with the literature[31]. The band gap of  $\text{Ag-WO}_3$  was calculated (Table 1) 2.68 eV and 2.45 eV before and after annealing respectively. The band gap tailoring was identified due to the morphology of CSNH and quantum confinement effect [34]. Interfaces of  $\text{Ag-WO}_3$  nanocubes heterostructures strongly affects the charge transfer and separation mechanisms[33]. This is due to the Ag nano-layer which is act as a localized surface plasmons (LSP). This separation mechanism attributes the electromagnetic waves to combine the electron oscillations[32]. And this process allows reducing the band gap (Figure, 8.) of the core cell structure. Subsequently, this tailoring band gap permits more visible light interaction with the CSNH than controlled  $\text{WO}_3$ . Tuning the band gap features, the CSNH reflects the promise of this heterostructures as a photocatalysis.

**Table 1.** Summary of the band gap analysis using UV-vis absorption

	Band Gap (eV)	Wavelength(nm)
$\text{WO}_3$	2.9	428
$\text{Ag@WO}_3$	2.68	464
Annealed $\text{Ag@WO}_3$	2.45	506

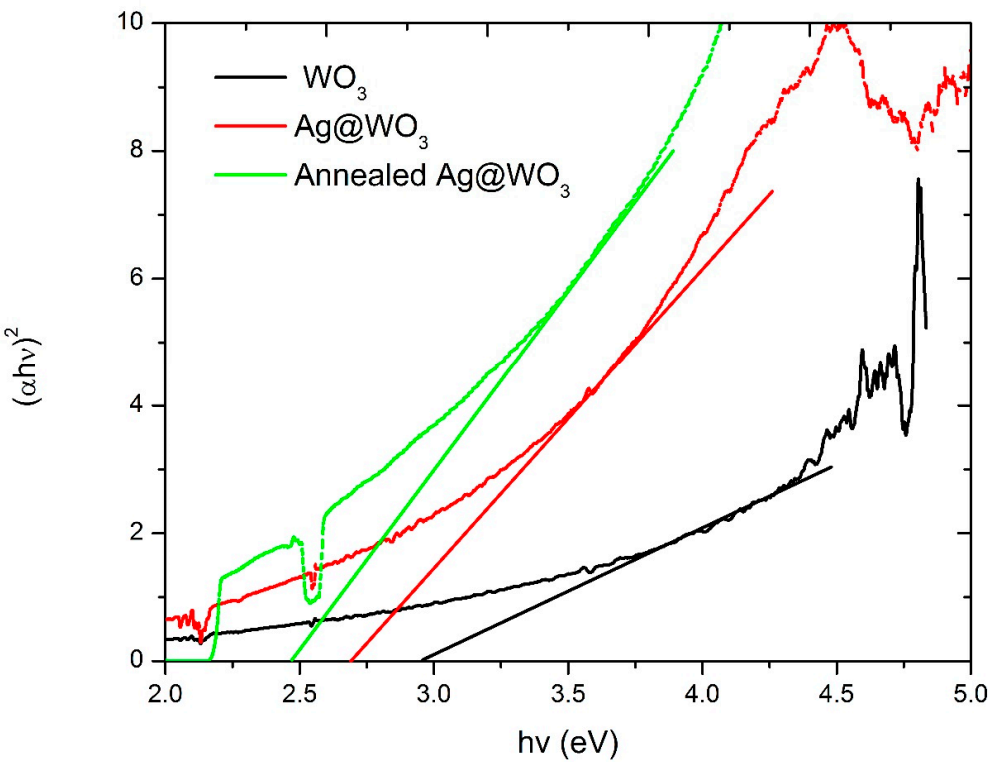


**Figure 7.** Band gap energy of  $\text{WO}_3$ ,  $\text{Ag-WO}_3$  before and after annealing using UV-vis absorption



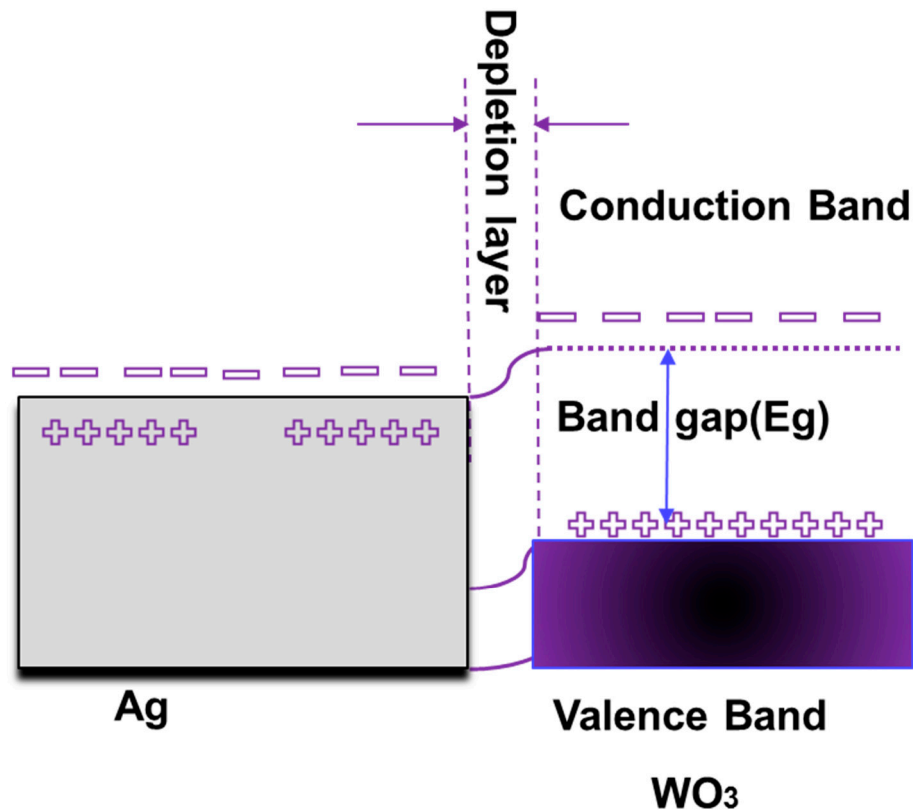


**Figure 8.** Band gap tailoring mechanism for Ag-coated WO<sub>3</sub> CSNH

#### 4. Conclusions

In summary, the study reports the fabrication of core-shell nano-heterostructures. The fabrication comprised of WO<sub>3</sub> nano-cubes coated with a thin shell of polycrystalline Ag avoiding all wet chemical routes. Sputtering of WO<sub>3</sub> was done on Si substrate, and then the thermal growth of WO<sub>3</sub> nanocubes was performed in a box furnace, and again Ag was coated on the surface of the WO<sub>3</sub> nanocubes by sputtering. The morphologies, interfaces, elemental analysis, crystal structures, phases and band gaps of the heterostructures were characterized using FESEM, EDX, XRD and UV-vis spectroscopic methods. FESEM images confirmed the particle size, morphologies of the WO<sub>3</sub> and the interfaces created between Ag and WO<sub>3</sub>. EDX supported the elemental analysis of CSNH. On top of that, XRD approved the crystallinity and monoclinic phase of WO<sub>3</sub> and presence of polycrystalline Ag coating. In conclusion, band gap analysis of Ag-WO<sub>3</sub> nano-cubes heterostructures exposed alterations of absorption peaks compare to pristine WO<sub>3</sub> nanocubes and band gap tailoring which could be accredited to the quantum confinement effects of heterostructures.

**Acknowledgments:** This work was sponsored by the National Science Foundation NSF-EPSCoR RII award (#24067). In addition, N. C. and M.I. thank the Graduate Council Fellowship (GCF) by the University of Alabama Graduate School. The authors express thanks to the Central Analytical Facility (CAF) at the University of Alabama for characterization.

**Author Contributions:** N. C. and M.I. designed the experiments; M.I. performed the experiments; N. C. and M.I. analyzed the data, M.I. wrote the paper

**Conflicts of Interest:** The authors declare no conflict of interest.



## References

- Hill, J. J.; Banks, N.; Haller, K.; Orazem, M. E.; Ziegler, K. J., An Interfacial and bulk charge transport model for dye-sensitized solar cells based on photoanodes consisting of core-shell nanowire arrays. *Journal of the American Chemical Society* **2011**, 133, (46), 18663-18672.
- Musin, R. N.; Wang, X.-Q., Structural and electronic properties of epitaxial core-shell nanowire heterostructures. *Physical Review B* **2005**, 71, (15), 155318.
- Danwittayakul, S.; Jaisai, M.; Dutta, J., Efficient solar photocatalytic degradation of textile wastewater using ZnO/ZTO composites. *Applied Catalysis B: Environmental* **2015**, 163, 1-8.
- Eriksson, J.; Khranovskyy, V.; Söderlind, F.; Käll, P.-O.; Yakimova, R.; Spetz, A. L., ZnO nanoparticles or ZnO films: A comparison of the gas sensing capabilities. *Sensors and Actuators B: Chemical* **2009**, 137, (1), 94-102.
- Lam, S.-M.; Sin, J.-C.; Abdullah, A. Z.; Mohamed, A. R., ZnO nanorods surface-decorated by WO<sub>3</sub> nanoparticles for photocatalytic degradation of endocrine disruptors under a compact fluorescent lamp. *Ceramics International* **2013**, 39, (3), 2343-2352.
- Tasaltin, C.; Ebeoglu, M. A.; Ozturk, Z. Z., Acoustoelectric effect on the responses of SAW sensors coated with electrospun ZnO nanostructured thin film. *Sensors* **2012**, 12, (9), 12006-12015.
- Xia, H.; Hong, C.; Shi, X.; Li, B.; Yuan, G.; Yao, Q.; Xie, J., Hierarchical heterostructures of Ag nanoparticles decorated MnO<sub>2</sub> nanowires as promising electrodes for supercapacitors. *Journal of Materials Chemistry A* **2015**, 3, (3), 1216-1221.
- Wang, X.; Liao, M.; Zhong, Y.; Zheng, J. Y.; Tian, W.; Zhai, T.; Zhi, C.; Ma, Y.; Yao, J.; Bando, Y., ZnO Hollow Spheres with Double-Yolk Egg Structure for High-Performance Photocatalysts and Photodetectors. *Advanced Materials* **2012**, 24, (25), 3421-3425.
- Habibi, M. H.; Habibi, A. H.; Zendeheel, M.; Habibi, M., Dye-sensitized solar cell characteristics of nanocomposite zinc ferrite working electrode: Effect of composite precursors and titania as a blocking layer on photovoltaic performance. *Spectrochimica Acta Part A: Molecular and Biomolecular Spectroscopy* **2013**, 110, 226-232.
- Han, Z.; Liao, L.; Wu, Y.; Pan, H.; Shen, S.; Chen, J., Synthesis and photocatalytic application of oriented hierarchical ZnO flower-rod architectures. *Journal of hazardous materials* **2012**, 217, 100-106.
- Habibi, M. H.; Rahmati, M. H., The effect of operational parameters on the photocatalytic degradation of Congo red organic dye using ZnO-CdS core-shell nano-structure coated on glass by Doctor Blade method. *Spectrochimica Acta Part A: Molecular and Biomolecular Spectroscopy* **2015**, 137, 160-164.
- Eskizeybek, V.; Sarı, F.; Gülce, H.; Gülce, A.; Avcı, A., Preparation of the new polyaniline/ZnO nanocomposite and its photocatalytic activity for degradation of methylene blue and malachite green dyes under UV and natural sun lights irradiations. *Applied Catalysis B: Environmental* **2012**, 119, 197-206.
- Habibi, M. H.; Karimi, B.; Zendeheel, M.; Habibi, M., Fabrication, characterization of two nano-composite CuO-ZnO working electrodes for dye-sensitized solar cell. *Spectrochimica Acta Part A: Molecular and Biomolecular Spectroscopy* **2013**, 116, 374-380.
- Akhavan, O.; Choobtashani, M.; Ghaderi, E., Protein degradation and RNA efflux of viruses photocatalyzed by graphene-tungsten oxide composite under visible light irradiation. *The Journal of Physical Chemistry C* **2012**, 116, (17), 9653-9659.
- Habibi, M. H.; Rahmati, M. H., Fabrication and characterization of ZnO@CdS core-shell nanostructure using acetate precursors: XRD, FESEM, DRS, FTIR studies and effects of cadmium ion concentration on band gap. *Spectrochimica Acta Part A: Molecular and Biomolecular Spectroscopy* **2014**, 133, 13-18.
- Kavitha, T.; Gopalan, A. I.; Lee, K.-P.; Park, S.-Y., Glucose sensing, photocatalytic and antibacterial properties of graphene-ZnO nanoparticle hybrids. *Carbon* **2012**, 50, (8), 2994-3000.
- Habibi, M. H.; Karimi, B.; Zendeheel, M.; Habibi, M., Preparation of nanostructure mixed copper-zinc oxide via co-precipitation rout for dye-sensitized solar cells: The influence of blocking layer and Co (II)/Co (III) complex redox shuttle. *Journal of Industrial and Engineering Chemistry* **2014**, 20, (4), 1462-1467.
- Li, Y.; Zhang, W.; Niu, J.; Chen, Y., Mechanism of photogenerated reactive oxygen species and correlation with the antibacterial properties of engineered metal-oxide nanoparticles. *ACS nano* **2012**, 6, (6), 5164-5173.
- Montazerzohori, M.; Hosseini Pour, S. A., Photocatalytic decolorization of 5-[4-(dimethylamino) phenylmethylene]-2-thioxo-4-thiazolidinone using nano-powder zinc oxide at various basic buffer pHs. *Desalination and Water Treatment* **2014**, 52, (40-42), 7993-7998.



20. Habibi, M. H.; Mardani, M., Co-precipitation synthesis of nano-composites consists of zinc and tin oxides coatings on glass with enhanced photocatalytic activity on degradation of Reactive Blue 160 KE2B. *Spectrochimica Acta Part A: Molecular and Biomolecular Spectroscopy* **2015**, 137, 785-789.
21. Penza, M.; Milella, E.; Anisimkin, V., Monitoring of NH<sub>3</sub> gas by LB polypyrrole-based SAW sensor. *Sensors and Actuators B: Chemical* **1998**, 47, (1), 218-224.
22. Jakubik, W. P.; Urbańczyk, M. W.; Kochowski, S.; Bodzenta, J., Palladium and phthalocyanine bilayer films for hydrogen detection in a surface acoustic wave sensor system. *Sensors and Actuators B: Chemical* **2003**, 96, (1), 321-328.
23. Hejczyk, T.; Urbanczyk, M.; Jakubik, W., Semiconductor sensor layer in SAW gas sensors configuration. *Acta Physica Polonica-Series A General Physics* **2010**, 118, (6), 1153.
24. Jakubik, W. P., Hydrogen gas-sensing with bilayer structures of WO<sub>3</sub> and Pd in SAW and electric systems. *Thin Solid Films* **2009**, 517, (22), 6188-6191.
25. Saoud, K.; Alsoubaihi, R.; Bensalah, N.; Bora, T.; Bertino, M.; Dutta, J., Synthesis of supported silver nano-spheres on zinc oxide nanorods for visible light photocatalytic applications. *Materials Research Bulletin* **2015**, 63, 134-140.
26. Chopra, N.; Shi, W.; Bansal, A., Structural evolution and stability studies of heterostructures comprised of carbon nanotubes decorated with nickel/nickel oxide core/shell nanoparticles. *Carbon* **2011**, 49, (11), 3645-3662.
27. Patil, S. S.; Patil, R. H.; Kale, S. B.; Tamboli, M. S.; Ambekar, J. D.; Gade, W. N.; Kolekar, S. S.; Kale, B. B., Nanostructured microspheres of silver@ zinc oxide: an excellent impeder of bacterial growth and biofilm. *Journal of Nanoparticle Research* **2014**, 16, (11), 1-11.
28. Xu, L.; Yin, M.-L.; Liu, S., Superior sensor performance from Ag@WO<sub>3</sub> core-shell nanostructure. *Journal of Alloys and Compounds* **2015**, 623, (0), 127-131.
29. Zhou, X.; Hu, C.; Hu, X.; Peng, T.; Qu, J., Plasmon-Assisted Degradation of Toxic Pollutants with Ag-AgBr/Al<sub>2</sub>O<sub>3</sub> under Visible-Light Irradiation. *The Journal of Physical Chemistry C* **2010**, 114, (6), 2746-2750.
30. Xu, M.; Liang, T.; Shi, M.; Chen, H., Graphene-like two-dimensional materials. *Chemical reviews* **2013**, 113, (5), 3766-3798.
31. Huang, B.-R.; Lin, T.-C.; Liu, Y.-M., WO<sub>3</sub>/TiO<sub>2</sub> core-shell nanostructure for high performance energy-saving smart windows. *Solar Energy Materials and Solar Cells* **2015**, 133, (0), 32-38.
32. Xu, L.; Yin, M.-L.; Liu, S. F., Agx@WO<sub>3</sub> core-shell nanostructure for LSP enhanced chemical sensors. *Scientific reports* **2014**, 4, 4.
33. Shi, W.; Chopra, N., Controlled fabrication of photoactive copper oxide-cobalt oxide nanowire heterostructures for efficient phenol photodegradation. *ACS applied materials & interfaces* **2012**, 4, (10), 5590-5607.
34. Chopra, N.; Shi, W.; Lattner, A., Fabrication and characterization of copper oxide (CuO)-gold (Au)-titania (TiO<sub>2</sub>) and copper oxide (CuO)-gold (Au)-indium tin oxide (ITO) nanowire heterostructures. *Materials Characterization* **2014**, 96, (0), 71-77.



© 2017 by the authors; licensee Preprints, Basel, Switzerland. This article is an open access article distributed under the terms and conditions of the Creative Commons by Attribution (CC-BY) license (<http://creativecommons.org/licenses/by/4.0/>).